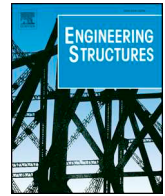




ELSEVIER

Contents lists available at ScienceDirect

Engineering Structures

journal homepage: [www.elsevier.com/locate/engstruct](http://www.elsevier.com/locate/engstruct)

# Statics of self-balancing masonry domes constructed with a cross-herringbone spiraling pattern

Vittorio Paris, Attilio Pizzigoni, Sigrid Adriaenssens

Street G. Marconi, 5, 240044 Dalmine, BG, Italy



## ARTICLE INFO

### Keywords:

Dome  
Vault  
Masonry  
Discrete element modelling  
Graphical analysis  
Self-balancing  
Plate-bande  
Herringbone

## ABSTRACT

The Brunelleschi herringbone pattern was certainly known by the Sangallo in the 16th century, who developed their own self-balanced construction technology for masonry domes based on the cross-herringbone spiraling pattern. Such technology was used for over one century in Italy to build masonry domes without shoring and formwork. However today it is not well known how this cross-herringbone spiraling pattern enables equilibrium states of self-balancing masonry domes. Therefore, in this study we demonstrate how this pattern permits equilibrium states of an octagonal masonry dome using two analysis approaches (i.e. Discrete Element Model and Limit State Analysis). The Discrete Element Model analysis has been performed to show the existence of the plate-bande resistance within the pattern. Even in the construction stages, these plate-bande resistance systems are capable of preventing sliding and overturning of the masonry dome. With the global self-balanced static equilibrium state proven, a Limit State Analysis is then adopted to estimate a possible thrust configuration needed to achieve equilibrium of the plate-bandes and the whole dome at each construction stage. It is shown that the value of the mortar friction has little influence on the static behavior of the dome. The study of the cross-herringbone spiraling pattern does not merely serve historical or conservation purposes. It has practical applications for the development of dry self-balanced robotic masonry construction technologies, particularly suited for unmanned aerial vehicles.

## 1. Introduction

Thin shell structures can define architectural forms and resist loads efficiently at the same time [1]. Yet the labor and materials involved in the installation of their formwork and shoring, needs to be of high quality and is therefore costly. Engineers, architects, and other building professionals are of the opinion that this high construction cost is the main obstacle for their larger adoption in the construction industry today [2]. Therefore, we investigate the equilibrium states of self-balancing domes, constructed with the cross-herringbone spiraling masonry pattern, to gain insight on how to build rigid structural surfaces without the need for formwork or shoring.

Throughout history, a number of construction technologies have enabled the realization of self-balancing curved rigid structural surfaces. In this paper, the terminology self-centering [3], self-supporting [4] or self-balancing [5] refers to the state of being in static equilibrium without the need for support formwork or shoring during all phases of construction. These terms can be used interchangeably and 'self-balancing' is used throughout this text from here onwards. Historic construction techniques that enable self-balancing domes and shells, include Nubian and Catalan masonry vaulting techniques [6] and Gothic

ribbed vaulting [7]. The focus of this paper is on the cross-herringbone spiraling masonry pattern as an enabler for a self-balancing construction technique of masonry domes or shells. This bricklaying pattern was developed by the Sangallo, building upon Brunelleschi's spiraling masonry technology [8,9]. Today a few built instances remain of the cross-herringbone technology: the most fascinating structures are the dome of the Simon Mago dome in Saint Peter cathedral (1530–1535, Rome) [10], and the Santa Maria in Ciel d'Oro dome (1525–1548, Montefiascone) [11] both designed by Antonio Sangallo the Younger and constructed by his brother [12]. These historic domes are double-layered. Our study focuses solely on the self-balancing construction of the interior dome which enables the erection of the outer dome. The cross-herringbone spiraling pattern is a masonry layout defined by a double loxodromic curves system, one left-handed and the one right-handed one. The resulting geometries depicted in Fig. 1, consists of intersecting spiraling loxodromic curves [13] (or rhumb lines which are basically curves crossing all meridians of longitude at the same angle [11]). This layout can be applied to a wide range of dome geometries such as hemispherical [10] or octagonal [12] forms. Scholars [11] have described the geometric principles that underlie the form description and the spiraling pattern layout of this cross-herringbone spiraling

E-mail address: [vittorio.paris@unibg.it](mailto:vittorio.paris@unibg.it) (V. Paris).

<https://doi.org/10.1016/j.engstruct.2020.110440>

Received 13 August 2019; Received in revised form 2 January 2020; Accepted 26 February 2020

Available online 14 May 2020

0141-0296/ © 2020 The Authors. Published by Elsevier Ltd. This is an open access article under the CC BY-NC-ND license

(<http://creativecommons.org/licenses/by-nc-nd/4.0/>).

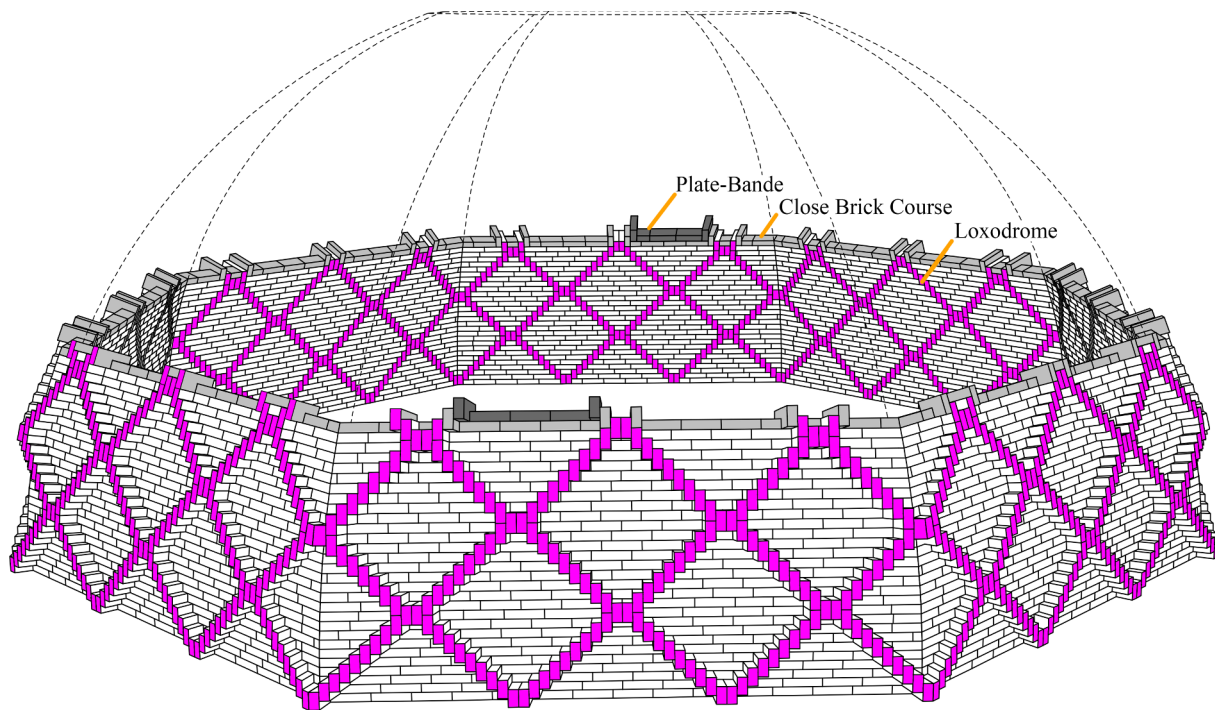


Fig. 1. Perspective of self-balancing dome under construction showing a plate-bande: (highlighted dark gray), closed brick course (highlighted light gray shaded) and left and right-handed loxodromic trajectories (highlighted purple). (For interpretation of the references to colour in this figure legend, the reader is referred to the web version of this article.)

based on the use of simple physical tools such as ropes and wooden arches as guidelines. To understand the static behavior of the completed domes, one can rely on a long history of theories. For an extensive literature on the matter, the reader is referred to Fang [14]. At the core of the theories of interest to the presented work, lies Heyman's Limit State Analysis [15]. Heyman used this analysis to establish thrust lines and appropriate  $t/R$  ratios to study static equilibrium in completed masonry domes (where  $t$  is the thickness of the dome and  $R$  is the radius of the dome).

A graphic statics approach, presented by Eddy [16], led to the development of the Modified Thrust Line Method (MTLM) [17] which allows analysis of a dome through slices, within the Limit State Analysis.

The use of the Limit State Analysis applied to masonry structures under static [18–21], and seismic loading [22] has been widely published in recent years. Its validity has also been demonstrated by a number of full-scale vault experiments [23,24], in which the limit state analysis was key for the vault's form-finding process [25].

From a numerical perspective, Discrete Element Modelling (DEM) had been adopted for the analysis of masonry domes. Although DEM was initially developed to model the mechanics of rocks [26,27], Lemos and other researchers have proven its validity to simulate the static and dynamic behaviour of masonry structures [28–30]. To the best of the authors' knowledge, only one study has used DEM to analyse the structural behaviour of a completed herringbone spiraling dome, in particular using a numerical Non-Smooth-Contact-Dynamics approach: Beatini highlighted the forces in the completed herringbone spiraling dome [31]. In literature, few methods [3] have been presented to study the global static equilibrium state of self-balancing domes *under construction*. Using Limit State Analysis, the conditions to achieve states of self-balancing can analytically be defined by balancing the overturning moment and by preventing the slippage. Another graphic static approach to study states of self-balancing equilibrium in domes is the MTLM, which can be used to study the behaviour of completed domes. A few studies [5,8] suggest that the herringbone pattern enables the construction of self-balancing domes, but no published study has

proven this hypothesis. There is a clear gap of knowledge on how masonry domes constructed with a cross-herringbone spiraling pattern achieve equilibrium states through self-balancing throughout all stages of construction.

Due to effect of the local equilibrium state of a series of bricks (dark gray) located between two herringbone spiraling bricks (light gray), shown in Figs. 1 and 2, on the global static behaviour during the construction of the dome, the statics of such a local assembly of bricks needs to be investigated. We hypothesize that such an assembly behaves like a plate-bande (or also called a lintel arch or flat masonry arch whose extrados and intrados are rectilinear) [32].

The bricks have radial joints that converge in the center (in the case of a spherical dome: at the centroid of the dome). The plate-bande exerts a thrust on the arch buttresses, or in the case of the domes under study, on the cross-spiraling herringbone bricks (shown in light gray in Fig. 2). For an overview on the plate-bande behavior, the reader is referred to Heyman [32] and Huerta [33]. Heyman applied the Limit State Analysis to the statics behind the plate-bande and explained the behavior of flying buttresses, Gothic spires and rose windows. In this paper, Heyman's Limit State Analysis approach is used to account for the plate-bande effect of the local brick assembly on the global static behavior of domes under construction. The research goal of this paper is thus to demonstrate how the spiraling cross-herringbone masonry pattern, enables the static equilibrium of self-balancing domes during all construction stages and when completed.

The remainder of this paper is organized as follows: in Section 2, the structural geometry, the methods and approach to demonstrate the



Fig. 2. Elevation of local brick Plate-Bande assembly consisting of a series of bricks (dark gray) and herringbone bricks (light gray).

validity of the hypothesis of the self-balancing cross-herringbone spiraling construction technology are presented. In Section 3, a detailed overview of the Heyman's Limit analysis used to evaluate the state of the cross-herringbone spiraling dome, is provided, as well as the assumptions under which the numerical simulations have performed are outlined. The results are summarized, compared and contrasted in Section 4. Conclusions about self-balancing and distribution of forces calculated are drawn in Section 5 and it is suggested how these patterns could be employed for self-balancing design and automated construction of contemporary domes using form-finding techniques and robotic construction.

## 2. Material and method

### 2.1. Geometry

The analysis conducted in this paper has been applied to an octagonal dome with a maximum radius of the circumscribed circle of 4 m. However different dome shapes can be evaluated using the same approach [11]. The octagonal geometry of this structure under study consist of eight identical cylindrical sails, with zero Gaussian curvature. It has been chosen for analysis as no self-balancing construction technologies are known to exist for the realisation of domes with this shape. To this dome, a cross-herringbone spiraling pattern is applied. As shown in Fig. 1, this pattern consists of an arrangement of horizontal brick courses which are interrupted by vertical herringbone bricks. The herringbone bricks are laid in regular intervals and placed at the same plane to the horizontal bricks: they are arranged in a radial manner. This geometric property is key to understanding the structural behaviour of the dome under construction. The herringbone geometry described by this brick layout results in a loxodromic curve, whose inclination is a function of the ratio of the vertical and horizontal mortar joint thickness as well as the dimensions of the brick.

The cross-herringbone spiraling pattern is a double system of herringbone paths, one of them is constituted by left-handed spirals and the second by right-handed curves. The nodes, highlighted in Fig. 3 (left), defined through the intersections of the loxodromic curves are materialized by herringbone bricks laid side by side. When a spiral intersects the sail edge, the spiral is terminated and another herringbone spiral begins in the next sail. Since all the spiral paths have the same inclination on the sail's boundary, irregular spatial nodes arise. The brickwork appears as a complex system of rhombi, shown in Fig. 3 (right), each one is bounded by spiraling paths. From the bottom to the crown of the dome, the size of the rhombi decreases. Near the dome

ribs, the rhombi are defined through paths which lie in the two different sails.

### 2.2. Method

Two different types of analysis are adopted to study the equilibrium states of the spiraling cross-herringbone dome: one based on the limit state analysis and the other based on discrete element modelling. The Limit State Analyses is used to study local (thrust line method) and global (modified thrust line method) equilibrium states of the dome. The results of these limit state analyses are validated using discrete element modelling.

To investigate the equilibrium of the dome, two methods of the limit state analysis are employed, one using the thrust line method (TLM) and the other one using the modified thrust line method (MTLM [16,17]). Three necessary assumptions, formulated by Heyman, are made for these Limit State Analyses: (a) sliding of the bricks cannot occur, (b) the masonry has no tensile strength, and (c) the masonry has infinite compressive strength [34]. Generally speaking, completed masonry domes experience meridian compressive stresses of one order of magnitude lower than the masonry's crushing strength. The hoop forces experienced in a completed self-balanced dome, are generally low. However, it will be shown in Section 4 (Table 2), that during construction their value might be larger than the ones experienced in the completed dome. Consequently, for this study, the assumption of infinite compressive strength (assumption (c)) is valid as the internal compressive stresses are very low. Under construction, when the brick is being laid, sliding may occur, but even if, after assessment the motion stops, thus to validate the role of cross-herringbone pattern, the first hypothesis (a) has been removed from our analysis. Finite values of friction angle are adopted, nevertheless as proven by D'Ayala and Casapulla [35], a unique solution exists and the Limit State Analysis could be applied. According to the Safe Theorem applied for masonry [34], equilibrium of the dome is guaranteed if a thrust line exists which lies entirely within the cross-section of the dome. Therefore, we adopted a two-stepped approach consisting of a local and a global equilibrium verification. We perform the TLM to verify the equilibrium state of the completed courses (local 1, see Fig. 5) and of the brick courses as they are being laid (local 2, see Fig. 7), while we verify the overall equilibrium of the dome under construction using the MTLM (global 1, see Fig. 9). The MTLM combines Heyman's theory and membrane theory [36]. It is based on Heyman assumptions, but to achieve the dome equilibrium, more assumptions are required. These assumptions are:

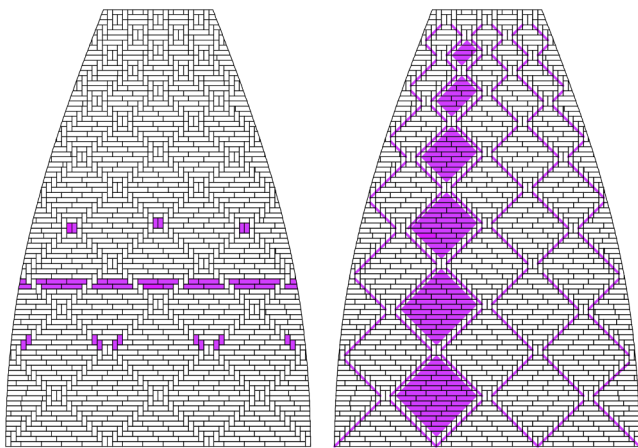


Fig. 3. Sail of an octagonal dome: brick pattern the elements highlighted: nodes (top), horizontal courses (middle), herringbone bricks (bottom) (left). Left and right-handed loxodromic curves (thick lines) and rhombi (areas filled) (right).

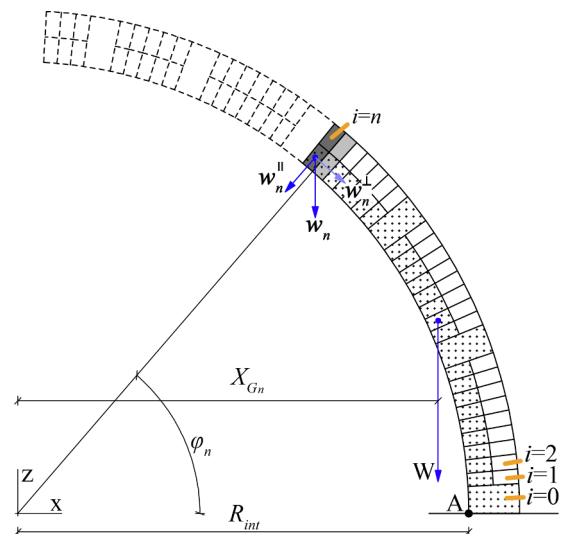


Fig. 4. Meridian section of dome: the incomplete voussoir arch.

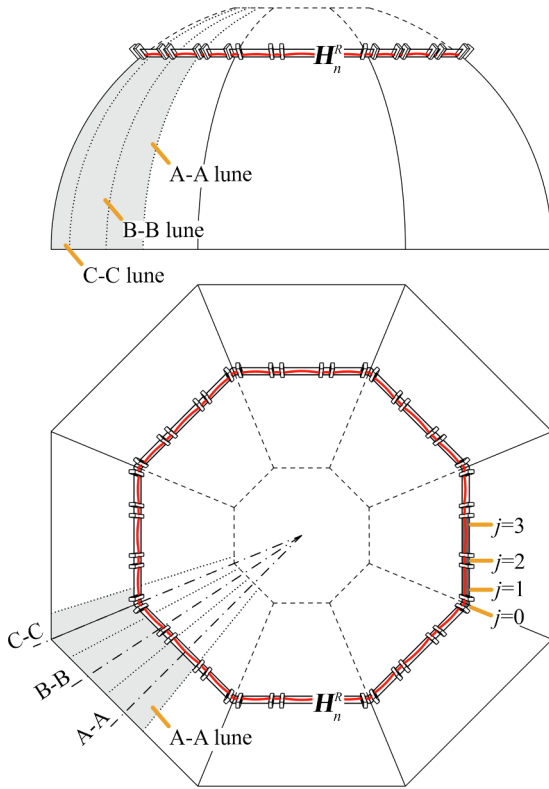


Fig. 5. Elevation (top) plan view (bottom). In the plan view: enumeration of plate-bands within a course, and closed brick course resulting in the  $n$ th compression ring (highlighted red). Lunes: A-A, B-B, C-C (plan view and elevation) and their middle section (plan view). (For interpretation of the references to colour in this figure legend, the reader is referred to the web version of this article.)

the load is uniform and axisymmetric, the hoop forces decrease from the crown to the base of the dome, unlike to meridional forces, which increase from crown to the base. Both the limit state methods (TLM (local 1 and 2), MTLM (global 1)) have been implemented for this study into the graphical editor algorithm Grasshopper [37] for Rhinoceros software [38].

The second one type of analysis used to evaluate the equilibrium states of the dome under construction has also been verified through a discrete element modelling numerical analysis. The dome analysed has been modelled in the commercially available software 3DEC (Itasca, Minneapolis, MN, USA.) [39] based on a Discrete Element Modelling (DEM) approach [40]. Discrete element methods can represent the behaviour of discontinuities and that of solid material, consequently they can describe the collapse of a masonry dome during construction. 3DEC software allows the evaluation of the structural behaviour of the dome through the explicit integration of the Newton's law of motion for a system of bodies whether they are deformable or rigid. The masonry has been modelled as a system of discrete rigid bodies (the bricks), and their interfaces as dry joints.

The analyses (DEM and Limit State) have been performed for different construction stages and structures namely for the plate-bande system, for the closed brick course, and for the dome in different phases of construction.

### 2.3. Approach

To understand how the cross-herringbone spiraling pattern allows the construction of a self-balancing octagonal dome, we need to analyse the different construction stages verifying the equilibrium of the simplified dome model adopted. To achieve this objective, the resistance

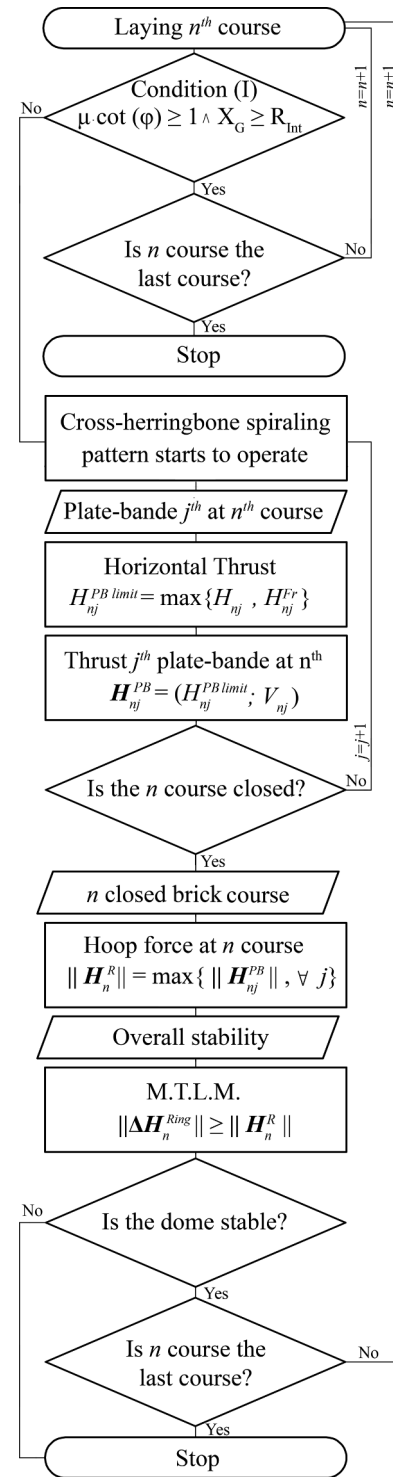


Fig. 6. Flow chart of equilibrium state analysis.

structure (global 1) and sub-structures (local 1 and 2) need to be assessed. The first sub-mechanism (local 1) manifests itself when the brick course is completed and the mason begins to lay a new course. The second sub-mechanism (local 2), the plate-bande system, occurs when the bricks are laid in a course which is not yet closed. Both systems are illustrated in Fig. 1. In this study both brick laying phases have been modelled at different heights corresponding to distinct construction stages, meanwhile, the overall stability of the dome has also been performed to ensure a full verification of the local and global equilibrium states.

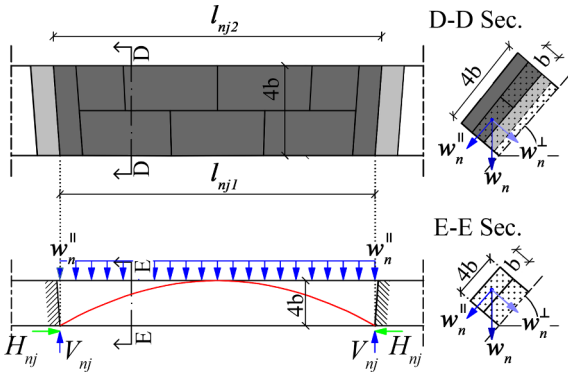


Fig. 7. Plate-bande at  $n$ th course plan view (left) and section (right), the graphical representation (top) and free body diagram (bottom).

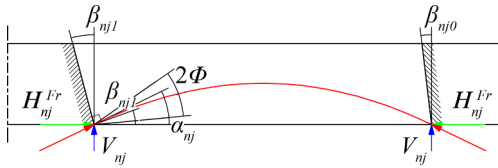


Fig. 8. Plate-bande. Angles:  $\alpha$ ,  $\beta$  and  $\Phi$  and a thrust line.

### 3. Theory

As discussed in Section 2, we propose a two-phase approach to verify the local and global stability of the dome under construction.

Under construction, the local equilibrium state of a self-balancing cross-herringbone spiraling dome is characterized by two resistance structures: the closed course structure (local 1) and the plate-bande structure (local 2). In this study, it is assumed that the octagonal dome is built through complete courses, only when the previous course is completed, the mason begins to lay a new course of bricks. Thus, any meridian section of the dome, evaluated during the construction stage, can be represented by an incomplete voussoir arch shape. Referring to Fig. 4, it is assumed that the voussoir bricks are rigid bodies with a mass. We further assume that they experience friction along their interfaces and that they can slip as a rigid body on an inclined plane leading to overturning of the incomplete voussoir arch. Adopting the system reference  $O, X, Z$ , two equilibrium equations are distinguished: the first one relates to the local equilibrium of closed course mechanism (local 1). The second one considers the overturning moment of the constructed portion of the sail (global 1). Using Coulomb's law of friction, the first equilibrium equation can be expressed as:

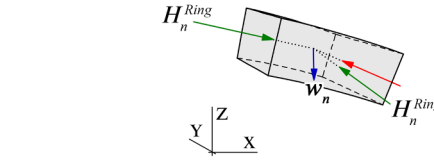
$$\begin{aligned} w_n^{\parallel} &= \|w_n\| \cdot \sin \varphi_n \\ w_n^{\perp} &= \|w_n\| \cdot \cos \varphi_n \\ \mu \cdot w_n^{\perp} &\geq w_n^{\parallel} \\ \mu \cdot \cot \varphi_n &\geq 1 \end{aligned} \quad (1)$$

where  $w$  is the weight of the bricks,  $\mu$  the mortar friction coefficient, while  $\varphi$  angle represents the inclination of the laying plane with respect to the horizontal plane and the  $n$  subscript denotes the last course, i.e.  $n$ th identifies the construction stage. As shown in Fig. 4, the  $i$  index corresponds to the course label, hence the first course built, it is denoted with  $i = 0$  index and the second  $i = 1$ , thus each course is uniquely defined by  $i$  and  $n$  defines the constructive stage. The second equation of equilibrium which relates to the overturning moment of the incomplete voussoir arch about its springing is formulated as:

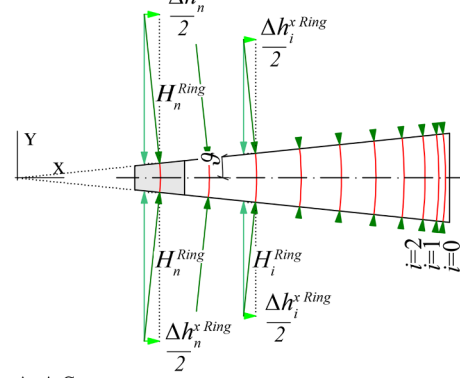
$$X_{Gn} \geq R_{int} \quad (2)$$

where  $X_{Gn}$  is the  $x$  coordinate of the centroid of incomplete voussoir arch, in the  $(O, X, Z)$  reference system, and  $R_{int}$  is the distance from the

### First block element



### A-A Lune



### A-A Sec.

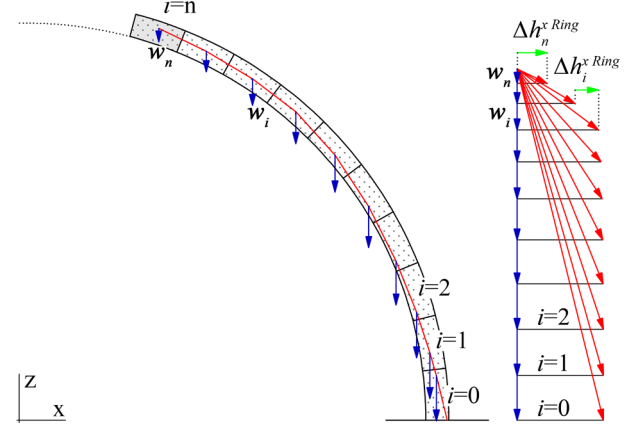


Fig. 9. MTLM for A-A lune at  $n$ -stage: equilibrium of the  $n$ th wedge-shaped element (top), plane view of A-A lune and ring forces (center), A-A section and thrust line (bottom).

origin to the center of rotation of the voussoir arch (or springing). Only if both inequalities, expressed in Eqs. (1) and (2) are verified, the system of rigid bodies (being the individual bricks and the constructed portion of the sail) is self-equilibrated. This can be expressed as:

$$\mu \cdot \cot \varphi_n \geq 1 \wedge X_{Gn} \geq R_{int} \quad (I)$$

Otherwise, if at least one of the two inequalities, (1) and/or (2), is not satisfied, the system of rigid bodies is not able to guarantee a self-balanced state. This can be expressed as (II):

$$\mu \cdot \cot \varphi_n \leq 1 \vee X_{Gn} \leq R_{int} \quad (II)$$

In the second case (II) to achieve a balance state, a system of auxiliary forces must be considered. The role of the cross-herringbone spiraling pattern is to provide this auxiliary force system through plate-bande action (local 2) to achieve the self-equilibrated state. As can be seen from the masonry pattern shown in Fig. 1, the realisation of the plate-bande action relies on the construction of complete horizontal brick courses, shown in Fig. 5, and on the radial arrangement of the cross-herringbone bricks shown in Fig. 7. The role of the cross-herringbone pattern can be derived by observing the physical behaviour of brick courses in the different construction stages. We define the last course ( $i = L$ ) as the first brick course in which the friction forces

between the bricks are not sufficient to avoid slippage (II). At the limit course ( $i = L$ ) the bricks slide towards the centroid of the dome. However, the presence of the herringbone bricks in the spiraling pattern, prevents them from slipping inwards. When the bricks of the limit course try to slip, they collide against the herringbone bricks, which are laid in a radial manner and fixed into the lower course ( $i = L-1$ ). This lower brick course is closed and the herringbone bricks at course ( $i = L$ ) are wedged into that lower brick course so that no sliding of the herringbone bricks can occur.

Even if the bricks of the lower course ( $i = L-1$ ) try to slide, the same mechanism will take place in the previous course ( $i = L-2$ ). Within the courses, plate-bande systems may be identified. Each of these plate-bande systems is bound by two herringbone bricks fixed into the lower course. The plate-bande systems act to prevent the failures by exerting a thrust against the herringbone bricks which transmit that thrust to the lower completed brick courses. Therefore, even in the second case (II) where the rigid bodies themselves are not sufficient to ensure a state of stable equilibrium, the cross-herringbone spiraling pattern provides internal supports so that the dome can be in equilibrium (local 2). These conclusions are further supported by the interpretation of the results of the DEM analysis reported in Section 4. Therefore even during the construction, the equilibrium of the masonry dome can be achieved through different systems: in the initial stages of construction equilibrium is provided by the system of friction forces (I). When these are not sufficient (II), the cross-herringbone spiraling pattern starts to operate, the structures of the closed brick courses (local 1) and the plate-bandes (local 2) provide the auxiliary forces required to maintain the static equilibrium of the dome under construction.

### 3.1. Thrust limit analysis

To uniquely identify the brick courses the subscript  $i$  has been assumed, but within each course, several plate-bande structures exist. Therefore as shown in Fig. 5, to identify every plate-bande structure, the  $j$  subscript has been adopted. Considering one of any course and referring to Fig. 5,  $j$  is equal to zero at the south edge of the east sail of the dome,  $j$  increases in a right-handed manner.

The process which has been developed to perform the equilibrium state analysis of the dome (both local and global) under all construction stages, is summarized in the flowchart in Fig. 6. First of all, for each  $n$ th constructive stage it is verified whether the bricks are self-balanced (I) then analyses are performed to assess the state of each structure namely the plate-bande, the closed brick courses and the constructed portion of the dome. Thereafter all  $j$  plate-bandes at the laying course are evaluated. Once the thrust of all plate-bandes in that laying course is computed, the stability of the compressive rings of the underlying closed brick course is verified and finally the overall equilibrium of the dome is verified using MTLM This approach, illustrated in Fig. 6, is repeated for all construction stages until the last course is laid.

#### 3.1.1. Plate-bande

The plate-bande is a straight arch. Because of its geometry, it is impossible to find a collapse mechanism. Hence the maximum thrust of the plate-bande structure is related to the crushing strength of the bricks. The thrust of plate-bande can be defined through considerations of equilibrium. We have adopted two formulations: both do not consider friction on the laying plane (i.e. the bricks are laid onto a smooth surface). This is a conservative assumption, in reality, the bricks would be posed onto a mortar bed which provides frictional resistance. The first formulation, respects Heyman's assumptions, (a) and (c) discussed in Section 2. The limit thrust is related to the loads applied, the length, and thickness of the plate-bande [31]. The length of plate-bande is a function of its location in the dome (i.e. the higher up in the dome, the smaller its length) and it also depends on its position within the course. We define the brick dimensions as multiple of  $b$ :  $b$  the height,  $2b$  the width and  $4b$  the length (in the model  $b = 6$  cm) and the  $\rho$  density of

bricks. The  $H$  horizontal thrust and  $V$  the vertical thrust are evaluated through the equilibrium equations (5) and (6).

$$w_{nj}^{\parallel} = 2 \cdot (l_{nj1} + l_{nj2}) \cdot b^2 \cdot \rho \cdot \sin(\varphi_n) \quad (3)$$

$$H_{nj} = \frac{w_{nj}^{\parallel} \cdot l_{nj1}}{32 \cdot b} \quad (4)$$

$$H_{nj} = \frac{(l_{nj1} + l_{nj2}) \cdot l_{nj1} \cdot b \cdot \rho \cdot \sin(\varphi_n)}{16} \quad (5)$$

$$V_{nj} = (l_{nj1} + l_{nj2}) \cdot b^2 \cdot \rho \cdot \sin(\varphi_n) \quad (6)$$

Referring to  $n$  time of posing, the loads carried by the plate-bande are derived from the component of self-weight parallel to the laying plane as illustrated in Fig. 7.

The other approach is obtained by assuming a finite friction angle without sliding. To differentiate the horizontal thrust considering this quantity with respect to the horizontal thrust calculated by Eq. (5) based on the assumption of Heyman of infinite friction, the  $Fr$  in apex is adopted. Using Eq. (9), it is possible to evaluate the  $H^{Fr}$  horizontal thrust, which is defined by taking into account the friction between the faces of herringbone bricks. As shown in Fig. 7, the herringbone bricks have a radial arrangement, they have their long side not running parallel to the normal of the imaginary surface of cylindrical sail. Hence, referring to Fig. 8,  $\beta$  angles are defined. These, angles are bound by the normal of the imaginary surface of the cylindrical sail and the long side of herringbone bricks,  $\phi$  is the friction angle and the  $\alpha$  angle which describes the inclination of the thrust with respect to intrados of the sail (7). To avoid sliding of the bricks, the  $\alpha$  angle must be smaller or equal to the angle defined by  $\phi$  and  $\beta$  (8).

$$\tan(\alpha_{nj}) = \frac{V_{nj}}{H_{nj}^{Fr}} \quad (7)$$

The maximum horizontal thrust which prevents slipping can be determined by Eq. (9).

$$\alpha_{nj} \leq \phi + \beta_{nj} \quad k = (0, 1) \quad (8)$$

$$H_{nj}^{Fr} = \frac{(l_{nj1} + l_{nj2}) \cdot b^2 \cdot \rho \cdot \sin(\varphi_n)}{\tan(\phi + \beta_{nj})} \quad k = (0, 1) \quad (9)$$

Hence, the limit horizontal thrust in the plate-bande at the time of laying the bricks can be defined as the maximum horizontal thrust (10) required by the two approaches expressed in Eqs. (5) and (9), thus:

$$H_{nj}^{PB \text{ limit}} = \max\{H_{nj}, H_{nj}^{Fr} \quad \forall k\} \quad (10)$$

At the sail edges, where the two laying planes intersect each other and result in a geometric discontinuity (or fold line), a component of the thrust of the plate-bande pushes the dome outwards. However, due to the symmetry of the dome about that fold line and due to the loads, which are of a modest order of magnitude, the outward thrust does not expel the bricks on the fold line, thus it does not lead to failure of the dome. The  $H^{PB}$  thrust which acts on herringbone bricks laying on the previous layer is defined as:

$$H_{nj}^{PB} = (H_{nj}^{PB \text{ Limit}}, V_{nj}) \quad (11)$$

#### 3.1.2. Closed brick course

At the  $n$ th construction stage, once the entire  $n$ th bricks course is completed, a spatial compression ring is formed as shown in Fig. 5 (highlighted red). The magnitude of the ring force is estimated as the maximum thrust present in all the plate-bande structures at  $n$ th course or:

$$\|H_n^R\| = \max\{\|H_{nj}^{PB}\|, \quad \forall j\} \quad (12)$$

When the next course is positioned ( $n + 1$ ), the value of compression force in the  $n$ th completed ring and in the underlying completed

rings decrease, this is due to the beneficial effect of the weight of the upper brick courses. Thus, the value of compression force defined equation (12) is the maximum recorded during all construction stages of the dome. To determine the ring compression forces, other approaches could be assumed. For example, the contribution of the normal component of the self-weight of the bricks can be considered, in such manner the friction forces increase and the compression forces required to prevent sliding or overturning decrease. Or one could also evaluate the variation of the plate-bande horizontal thrust caused by the slight incline of the herringbone bricks during the laying of bricks, and its effect on the underlying closed brick courses. However, due to hyperstatic nature of the closed brick courses, all approaches proposed under the assumed hypotheses, do not allow for the quantitative definition of equilibrium state of the rings, but only give a qualitative definition.

Eq. (12) does allow us to compute the compression force value in the ring at the  $n$ th course at the  $n$ th constructive stage.

### 3.1.3. Overall stability

The compressive forces in the closed bricks courses act as hoop forces in domes of revolution, thus to evaluate the overall stability of the dome it is possible to assume the existence of a balance surface. Such surface depends on the compressive forces of the closed brick courses and on the vertical component of brick's self-weight.

To estimate the balance surface, we adopt MTLM As shown in Fig. 5 (lunes representative A-A, B-B, C-C) the octagonal dome is sliced by meridian planes into 32 lunes, in a manner so that for example the A-A section of A-A lune lies in the plane of symmetry of the sail. The balance surface is identified through the thrust traced in all different sections (e.g. sections A-A, B-B, C-C in Fig. 5) one for each different lune, thus the thrust in all different sections needs to be assessed.

As denoted in Section 3.1.2, the compression ring force of each closed brick course is constant, exactly as the hoop forces in domes of revolution. Therefore to trace the thrusts, one per section, the same distribution of compressive forces must be considered. In domes of revolution under axisymmetric loads, the geometry of the hoop forces are described by circles, thus the hoop force can be described through their  $\Delta h^{x Hoop}$  x-component and the  $\theta$  angle (13), which is the half angle defining a lune measured on horizontal plane as shown in Fig. 9.

$$\|H_i^{Hoop}\| = \frac{\Delta h_i^{x Hoop}}{2 \cdot \sin(\theta)} \quad (13)$$

However in the octagonal dome under study, the actual geometry of rings compressive forces is not known: they are affected by dome's geometry and by bricks pattern. Even from observing the spans of plate-bande structures, whose lengths vary from course to course it is clear that the shape of ring forces is affected by their shape.

Thus, we make the assumption in our analysis that the ring forces  $H^{Ring}$  act normal to the lunes side faces, namely, the  $\times$  component of ring forces can be described by the relation (14).

$$\Delta h_i^{x Ring} = 2 \cdot \|H_i^{Ring}\| \cdot \sin(\theta) \quad (14)$$

This adopted relation does not rely on the description of the actual geometry of ring forces, but it is based on the principle of equilibrium. According to the Safe Theorem [34], the real shape of the compressive rings is not significant, as long as the thrust line of the ring lies entirely within the thickness of the brick courses.

To prove the stability of dome under construction, we compute the thrust at different construction stages. For each construction stage, the thrust line has been evaluated, at first the section A-A, shown in Fig. 9, subsequently, for sections B-B and C-C at the same construction stage (sections A-A, B-B, C-C are referred to Fig. 5). To calculate the thrust for sections B-B and C-C, the same distribution of ring forces found in section A-A is assumed.

At the  $n$ th constructive stage, to guarantee that the ring forces are

sufficient to provide the forces required to achieve a stable equilibrium state of the  $n$ th closed bricks course, the inequality (15) must be satisfied:

$$\|H_n^{Ring}\| \geq \|H_n^R\| \quad (15)$$

Therefore, if all thrusts are compatible with the prescriptions of the Safe Theorem and inequation (15) is verified, it is proven that the dome is in a state of stable static equilibrium.

### 3.2. Discrete element model

As mentioned in Section 2.2 the bricks have been modelled as discrete rigid bodies, whose sizes correspond to brick dimensions ( $b$ ,  $2b$ ,  $4b$ ) plus the thickness of the mortar joint. As a realistic mortar joint does not have a constant thickness, the rigid bodies are slightly different from each other as their shape depends on the position of brick course within the whole dome and the brick position within the brick course. Due to the assumption of rigid bodies, the joints located at the interfaces of the discrete bodies have the physical meaning of representing the deformations and displacements of the mortar layers and the masonry bricks.

The failure Mohr-Coulomb model with zero tensile capacity and zero cohesion has been adopted in this study. Therefore the joints are characterized only by joint stiffness parameters:  $JK_n$ ,  $JK_s$  and the coefficient of Coulomb-friction. As described by Bagi [41],  $JK_n$ ,  $JK_s$  are related, respectively to the difficulty of pressing and slipping of the blocks with respect to each other. DEM analyses have been performed to prove the existence of the plate-bande and closed brick course structures. To understand the dome's structural behaviour during construction, several plate-bande structures located in different courses have been assessed. Each plate-bande structure has been modelled as an assembly of free rigid bodies (shown as blues in Fig. 10) laid onto a constrained underlying brick course (shown as green in Fig. 10).

The global equilibrium has been assessed simulating the constructive process, i.e. adding one course upon another. Once the overall equilibrium state has been reached for a given completed course, the next one is added and analysed to assess the overall stability of the dome.

## 4. Results

All analyses (plate-bande structure test, closed brick courses test and overall stability test) have been performed for the self-weight of the bricks only considering a material density equal to  $\rho = 2500 \text{ kg/m}^3$  and the gravitational acceleration  $g = 9.81 \text{ m/sec}^2$ . The values of the joint stiffness parameters:  $JK_n$ ,  $JK_s$  change for the different tests. To evaluate the stability of the plate-bande structures, they are assigned the values 100 GPa/m and 10 GPa/m based on [40]. A variety of  $\Phi$  friction angles has been considered ( $0^\circ$ ,  $10^\circ$ ,  $15^\circ$ ,  $20^\circ$ ,  $40^\circ$ ,  $60^\circ$ ,  $80^\circ$ ,  $90^\circ$ ).

The results of the plate-bandes tests show that the stability of plate-bandes is related to the friction angle  $\Phi$  and to the angle of inclination

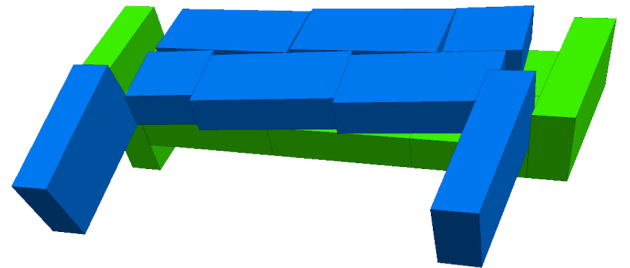


Fig. 10. Test on plate-bande  $n = i = 58$ ,  $j = 2$  and  $\Phi = 0^\circ$ . The free blocks (blue) slide on the constrained elements (green). (For interpretation of the references to colour in this figure legend, the reader is referred to the web version of this article.)

**Table 1**  
Stability (Yes/No) of completed courses at different construction stages for an angle of friction  $\Phi = 10^\circ$  and  $\Phi \geq 15^\circ$ .

Course $i$	$\Phi = 10^\circ$				$\Phi \geq 15^\circ$			
	Stage $n$				Stage $n$			
	36	58	89	93	35	58	89	93
36	Yes	Yes	No	No	Yes	Yes	Yes	Yes
58		Yes	No	No		Yes	Yes	Yes
89			No	No			Yes	Yes
93				No				Yes

of laying plane. In particular, if the friction angle  $\Phi$  is equal or larger than  $10^\circ$ , the plate-bande structures are stable. The results also show that for low and medium angles of inclination of the laying plane (that is up to the  $j$  36th brick course) the equilibrium of plate-bandes structures is not related to the friction angle  $\Phi$ .

To demonstrate the stability of the complete courses, a series of stability simulations is performed at  $n = 36, 58, 89$  construction stages observing the same physical properties as for the plate-bande structures analyses. Therefore, the closed bricks course test consists of evaluating the portion of the dome until the  $n$ th constructive stage. For example, to prove the stability of the 36th complete course, 36 complete courses have been modelled, and the maximum displacement and velocity of the bricks in 36th course have been recorded. Only the first laying plane has been constrained and none of the other bricks. As discussed in Section 3.2, for each construction stage, the upper course is only added when the previous course has found its equilibrium state.

Assuming the same physical properties, the structural behaviour of the whole dome is assessed (overall stability test), all 93 courses are modelled ( $n = 93$ ), but unlike the closed brick course tests, the displacements and velocities have been recorded at several courses. Table 1 summarizes the stability of the completed brick course and the whole dome related to the friction angles, the tests have executed to the same variety of values of friction adopted for plate-bande tests namely for  $\Phi = 10^\circ$  and  $\Phi \geq 15^\circ$ , and at several construction stages ( $n = 36, 58, 89, 93$ ).

Based on the results of the analysis for a wide range of friction angles and construction stages, a displacement surface for the bricks of

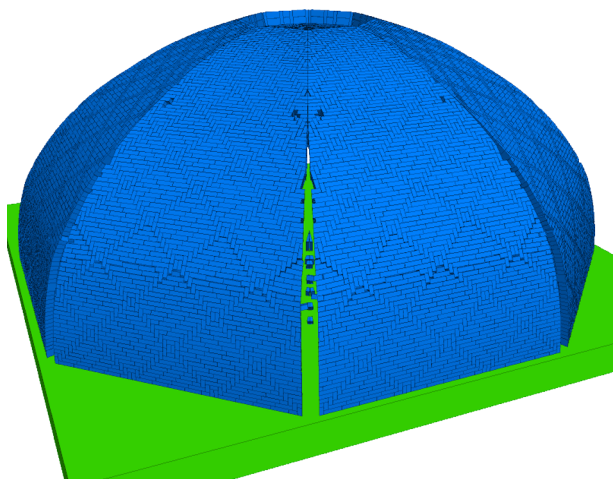


**Fig. 11.** Overall stability test,  $n = i = 93$  and  $\Phi = 10^\circ$ . The free blocks (blue) slide on the constrained elements (green). (For interpretation of the references to colour in this figure legend, the reader is referred to the web version of this article.)

a dome under construction can be shaped. Fig. 12 shows the surface of the displacements recorded at the 89th course and related to the constructive stages range  $n = 89-93$  and to the friction angles between  $\Phi = 10^\circ$  and  $90^\circ$ . Friction angles less than  $10^\circ$  have not been considered because even the plate-bandes structures are not stable at such low friction angles. Until the 88th construction stage, the dome displacement is less than 0.05 cm, thus the dome is stable even if the angle of friction is  $\Phi = 10^\circ$ . Then at the 89th construction stage, for angle of friction values of  $\Phi < 15^\circ$  the first courses slide on the fixed underlying plane, 8 slices are formed, one each sail (Fig. 11).

At the 90th stage, the openings located at sails edges reach the 30th course, then adding the next courses, they increase up to the 77th course. The dome stability is achieved when angle of friction  $\Phi$  is equal to or greater than  $15^\circ$ .

Referring to Fig. 12, DEM analyses point out that after an initial motion of the bricks, the plate-bande mechanism prevents any further motion even for real values of friction angle: even under construction no brick moves. For this reason, the Limit State Analysis can be applied to evaluate the two sub-mechanisms [42]. Therefore, once the stability of the dome under construction is proven, as described in Section 3.1, we perform TLN and MTLM For three different construction stages  $n = 36, 58, 89$  we determine the minimum thrust required to build the dome without any false or formwork. In Table 2 the values of thrust required to achieve the stability for the three different structures closed bricks course (local 1) and plate-bande structure (local 2) and the constructed portion of the dome (global 1), are reported.

As indicated in sections 3.0 and 3.1, the  $i$  and  $j$  indexes correspond to the course label and the plate-bande number within a course respectively. To perform the computation, the friction angle  $\Phi$  assumed is  $15^\circ$  because we have shown in this section that the friction angle value is the minimum angle that guarantees stability, see Table 1. While the geometry, the material density and inclination of laying plane are obtained from the model adopted for DEM analysis.

As expected, the thrust or ring forces, listed in Table 2, change as a function of the construction stage. For all construction stages the ring forces are larger near the last course laid than those located at the first level laid. Table 2 reports the x-component of ring forces at the 36th, 58th 89th construction stage, considering  $\Delta h_{36}^{x \text{ Ring}}$ . From the Table 2 it can be seen that the magnitude of ring forces required to achieve stability decreases drastically during construction. During the early construction stages, the magnitude of the ring forces is comparable to the thrust forces required to balance the plate-bandes, but near the crown, their magnitude increases independently of the plate-bandes thrusts.

This observed difference is due to the geometry and dimension of the plate-bande structure and of the entire dome. The spans of plate-bandes decrease from the base to the dome's crown by 84%, unlike the ring forces required to achieve a balanced state of the whole dome, which, at complete construction, increase from the base of the dome to the crown by as much as 98%.

The values of the incremental displacements are recorded in Table 3. These displacements are defined by considering their variation with respect to the completed course below. This displacement quantity is strictly related to the joint stiffness parameters ( $JK_n, JK_s$ , discussed in Section 3.2). Due to our choice of these parameters, the absolute magnitude of these displacements does not reflect the real one. Nevertheless, this quantity provides interesting notion insights on the dome behaviour under construction. As expected, during the construction stages, the displacement magnitudes change. All 3DEC simulations show that the maximum variation is recorded during the laying of the course  $i = 58$ th, corresponding to 53% completion of the entire dome. After that course and then for the following construction stages the incremental displacement decreases. When the dome is completed ( $n = 93$ ) the incremental displacement magnitude of the top course, in relation to the first course is 0.03 mm for  $\Phi = 15^\circ$  and 0.01 mm for  $\Phi = 90^\circ$ .

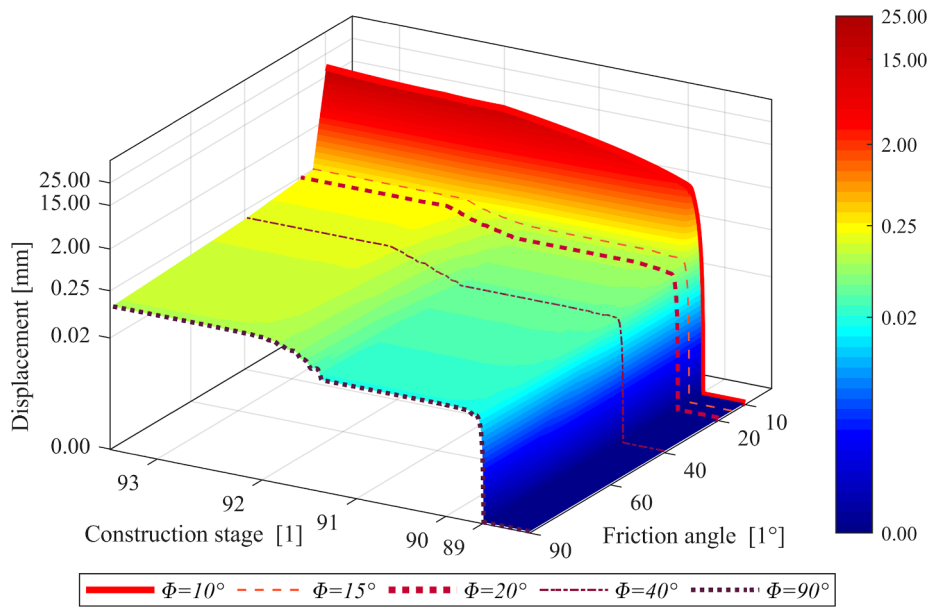


Fig. 12. Displacements surface related at the middle sail point at the 89th course.

Table 2

Thrust values for plate-bande structures, closed brick courses and portion of the dome for different construction stages obtained using Limit State Analysis (TLM and MTLM).

Plate-bande						
	Stage $n = i$					
	36		58		89	
$j$	0	2	0	2	0	2
$  H_n^{PB}  $ [N]	172.0	169.4	102.5	190.4	36.7	113.2
Closed brick course						
	Stage $n$					
	36		58		89	
$  H_n^R  $ [N]	169.4		190.4		113.2	
Portion of the dome						
	Stage $n$					
	36		58		89	
$\Delta h_{36}^{x Ring}$ [N]	130.0		30.1		2.9	
$\Delta h_{58}^{x Ring}$ [N]			230.0		16.9	
$\Delta h_{89}^{x Ring}$ [N]					280.0	
$  H_n^{Ring}  $ [N]	333.2		589.5		717.6	

Table 3

Magnitude of incremental displacement of middle sail point at courses  $i = 36, 58, 89$  and  $\phi = 15^\circ$ , ck courses and portion of the dome for different construction phases. Data obtained by DEM analysis.

Magnitude of Incremental Displacement [mm]			
Course $i$	Stage $n$		
	36	58	89
36	0.37	0.46	0.20
58		0.32	0.49
89			0.01

### 5. Conclusion

During the construction of masonry domes without shore or formwork, the overturning of a partially constructed sail and/or the sliding of local bricks or brick courses can lead to an unstable equilibrium state of the dome and ultimately structural failure. Traditional masonry construction technologies do not intentionally address such a construction failure mode and resort to costly auxiliary support systems.

The case study of an octagonal dome patterned with a spiraling cross-herringbone layout, proves that this brick layout enables self-balancing domes during all phases of construction without form or shoring. Through the plate-bande structures found in the incomplete brick course, a resistance mechanism is discovered that enables a self-balanced state by mobilising the underlying completed brick courses through the bonding with the herringbone bricks, linking new uncompleted course to the already completed underlying ones [8]. Once the brick course is closed, the plate-bandes structures are no longer necessary to sustain dome's stability, but instead they offer support to fix the herringbone bricks in the next course.

The existence of the plate-bande structures, the closed bricks courses and the stability of the dome under construction is demonstrated through the DEM analysis performed. As highlighted in Section 4, even for low values of friction between the brick surfaces, the dome finds a balanced equilibrium state.

For real friction angle values DEM analysis shows maximum displacements of only 0.25 mm. However of more relevance is the evolution of the motion of the bricks once the plate-bande and the closed brick course actions are mobilised. After that initial motion of the bricks, no further motion occurs and this for real values of friction angle. Therefore no brick moves even under construction.

Although the equations of equilibrium defined in Section 3.1 are used to verify the equilibrium state of the dome, they can be easily adapted to design self-balanced domes. Currently, three dimensional rigid structural surfaces (such as shells and domes) need formwork and shoring material during construction, which goes to waste once the entire structure is completed, adding to the economic and environmental cost of the project. In this paper, a historic masonry dome construction technique, based on the spiraling cross-herringbone pattern, has been shown to enable statically stable geometries throughout the construction process without the need for any external support system. These self-balancing structures have no theoretical limit to their

size. The disruptive potential of this historic masonry pattern comes to the fore for today's construction industry when this technology is viewed in the context of other emerging innovations such as novel structural form finding approaches and robotic construction technologies [43,44]. For example, it is envisaged that masonry rigid surfaces could be tailored in their shape through form-finding approaches [4,45,46] and patterned with the herringbone pattern to be effectively produced using aerial drones without any falsework and yet be stable during all stages of construction and their service life.

### Declaration of Competing Interest

The authors declared that there is no conflict of interest.

### Acknowledgements

The authors would like to thank dr. Rebecca Napolitano at Princeton University, dr. Rima Ghazal, dr. Nicola Lepore, Ph.D. student Alessandro Dell' Endice and Arch. Nandini Priya Thatikonda for the support provided during the study.

### Funding sources

This work was partially supported by the Ph.D. School of University of Bergamo, and the Princeton University International Fund at the Office for International Affairs and Operations at Princeton University. Software 3DEC was provided by Itasca C.G. under the Education Partnership Program for which the authors also express their gratitude.

### References

- [1] Lepore N. *Le volte in muratura: forma e struttura, equilibrio e analisi limite*. Roma Tre; 2018.
- [2] Meyer C, Sheer MH. Do concrete shells deserve another look? *Concr Int* 2005;43–50.
- [3] Oppenheim IJ, Gunaratnam DJ, Allen RH. Limit state analysis of masonry domes. *J Struct Eng* 1989;115(4):868–82.
- [4] Como M. Statics of historic masonry constructions, vol. 1; 2013.
- [5] Michiels T, Adriaenssens S. Form-finding algorithm for masonry arches subjected to in-plane earthquake loading. *Comput Struct* 2018;195:85–98.
- [6] Davis L, Ochsendorf J, Block P, DeJong M. Tile vaulted systems for low-cost construction in Africa. *ATDF J* 2010;7(1/2):4–13.
- [7] Wendland D. Traditional vault construction without formwork: Masonry pattern and vault shape in the historical technical literature and in experimental studies. *Int J Archit Herit* 2007;1(4):311–65.
- [8] Mainstone RJ. Brunelleschi's Dome of S. Maria del Fiore and some Related Structures. *Trans Newcom Soc* 1969;42(1):107–26.
- [9] Conti G, Corrazzi G. *The secret of Brunelleschi's Dome Florence*; 2011.
- [10] Zander G. Gli ottagonali di San Pietro riconosciute nel disegno Arch. *Uff. N. 1330. Palladio* 1998;1:62–82.
- [11] Docci M, Migliari R. La costruzione della spinapesce nella copertura della sala ottagonale di Simon Mago nella fabbrica di San Pietro. *Palladio* 1989;3(1989):61–72.
- [12] Pizzigoni A, Paris V, Pasta M, Morandi M, Parsani A. Herringbone naked structure. *Proc. IASS annual symposium. International Association for Shell and Spatial Structures (IASS)*; 2018.
- [13] Pizzigoni A, Paris V, Ruscica G. Herringbone technique: truth and history of a cutting-edge technology. *Proc IASS annual symposium. International Association for Shell and Spatial Structures (IASS)*; 2018.
- [14] Fang DL, Napolitano RK, Michiels TL, Adriaenssens SM. Assessing the stability of unreinforced masonry arches and vaults: a comparison of analytical and numerical strategies. *Int J Archit Herit* 2019;13(5):648–62.
- [15] Heyman J. On shell solutions for masonry domes. *Int J Solids Struct* 1967;3(2):227–41.
- [16] Eddy HT. *Researches in graphical statics*. D. Van Nostrand Publisher; 1878.
- [17] Lau WW. *Equilibrium analysis of masonry domes*. B.S.: Civil Engineering Michigan State University; 2006.
- [18] Lucchesi M, Padovani C, Pasquinelli G, Zani N. Static analysis of masonry vaults, constitutive model and numerical analysis. *J Mech Mater Struct* 2007;2(2):221–44.
- [19] Bergamasco I, Fortunato A, Gesualdo A, Iannuzzo A, Monaco M. AIMETA 2017 – Proceedings of the 23rd conference of the Italian association of theoretical and applied mechanics. 2017. p. 1430–8.
- [20] Cennamo C, et al. Rigid block for masonry. XXIII conference the Italian association of theoretical and applied mechanics. 2017. p. 1347–67.
- [21] De Chiara E, Cennamo C, Iannuzzo A, Angelillo M, Fortunato A, Gesualdo A, et al. Proceedings of the international masonry society conferences. 2018. p. 471–85.
- [22] Cusano C, Cennamo C, Angelillo M. Seismic vulnerability of domes: a case study. *J Mech Mater Struct* 2018;13(5):679–89.
- [23] Block P, Van Mele T, Liew A, DeJong M, Escobedo D, Ochsendorf J. Structural design, fabrication and construction of the Armadillo vault. *Struct Eng* 2018;96(5):10–20.
- [24] Block P, Rippmann M, Van Mele T, Escobedo D. The Armadillo vault balancing computation and tradition craft. *Fabricate* 2017. JSTOR; 2017. p. 286–93.
- [25] Block P, Lachauer L. Three-dimensional funicular analysis of masonry vaults. *Mech Res Commun* 2014;56:53–60.
- [26] Cundall PA. Formulation of a three-dimensional distinct element model—Part I. A scheme to detect and represent contacts in a system composed of many polyhedral blocks. *Int J Rock Mech Min Sci Geomech* 1988;25(3):107–16.
- [27] Hart R, Cundall PA, Lemos J. Formulation of a three-dimensional distinct element model—Part II. Mechanical calculations for motion and interaction of a system composed of many polyhedral blocks. *Int J Rock Mech Min Sci* 1988;25(3):117–25.
- [28] Çaktı E, Saygılı Ö, Lemos J. Discrete element modeling of a scaled masonry structure and its validation. Elsevier; 2016.
- [29] Psycharis IN, Lemos JV, Papastamatiou DY, Zambas C. Numerical study of the seismic behaviour of a part of the Parthenon Pronaos. *Earthq Eng Struct Dyn* 2003;32(January 2002):2063–84.
- [30] McInerney J, Dejong MJ. Discrete element modeling of groin vault displacement capacity. *Int J Archit Herit* 2015;9(8):1037–49.
- [31] Valentina B, Gianni R, Alessandro T. A non-smooth-contact-dynamics analysis of Brunelleschi's cupola: an octagonal vault or a circular dome? Elsevier; 2019. p. 1–23.
- [32] Heyman J. 'Gothic' construction in ancient Greece. *J Soc Archit Hist* 1972;31(1):3–9.
- [33] Huerta SF. Wedges and plate-bandes : mechanical theories after De la Hire. *L'architrave, le plancher, la plate-forme. Nouvelle Histoire de la construction*. Architecture Essais, vol. 1. Lausanne: Presses polytechniques et universitaires romandes; 2012. p. 405–35.
- [34] Heyman J. The stone skeleton. *Int J Solids Struct* 1966;2:249–79.
- [35] D'Ayala D, Casapulla C. Limit state analysis of hemispherical domes with finite friction. *Hist Constr Possibil Numer Exp Tech* 2001;1977:617–26.
- [36] Zessin J, Lau W, Ochsendorf J. Equilibrium of cracked masonry domes. *Proc Inst Civ Eng - Eng Comput Mech* 2010;163(3):135–45.
- [37] Davidson S. Grasshopper algorithmic modeling for rhino. Add-ons for Grasshopper. [Online]. Available: <https://www.grasshopper3d.com/> [accessed: 26-Dec-2019].
- [38] McNeel. Rhino 6 per Windows. [Online]. Available: <https://www.rhino3d.com/it/> [accessed: 26-Dec-2019].
- [39] 3DEC | US Minneapolis - Itasca Consulting Group, Inc. [Online]. Available: <https://www.itascacsg.com/software/3DEC> [accessed: 26-Dec-2019].
- [40] Manual, theory and background. Minneapolis (Minnesota, USA): Itasca Consulting Group. Inc.
- [41] Simon J, Bagi K. Discrete element analysis of the minimum thickness of oval masonry domes. *Int J Archit Herit* 2016;10(4):457–75.
- [42] De Serio F, Angelillo M, Gesualdo A, Iannuzzo A, Zuccaro G, Pasquino M. Masonry structures made of monolithic blocks with an application to spiral stairs. *Meccanica Jun.* 2018;53(8):2171–91.
- [43] Wendland D. *Lassaulx und der Gewölbekonstruktion mit selbsttragenden Mauerwerksschichten. Neumittelalterliche Architektur um 1825–1848*. VERLAG, MICHAEL IMHOF; 2008.
- [44] Bock T, Linner T. *Robotic industrialization*. Cambridge University Press; 2015.
- [45] Richardson JN, Adriaenssens S, Filomeno Coelho R, Bouillard P. Coupled form-finding and grid optimization approach for single layer grid shells. *Eng Struct* 2013;52:230–9.
- [46] Adriaenssens S, Block P, Veenendaal D, Williams C, editors. *Shell structures for architecture: form finding and optimization*. Routledge; 2014.